Nanotomography based study of gas diffusion layers

H. Ostadi, K. Jiang

Centre for Biomedical and Nanotechnology, School of Mechanical Engineering, University of Birmingham, Birmingham B15 2TT, UK

P. Rama, Y. Liu, R. Chen,

Dept. of Aeronautical and Automotive Engineering, Loughborough University, Leicestershire LE11 3TU, UK

X. Zhang,

Department of Engineering, University of Liverpool, Brownlow Street, L69 3GH, UK

Abstract

Nano-computed tomography (nanoCT) was used for non-invasive 3D visualization and characterization of porous gas diffusion layer (GDL) for polymer electrolyte membrane fuel cells (PEMFC). The study was conducted using reconstruction of 3D images of a GDL of polymer electrolyte fuel cell to determine the critical nanostructural parameters of the layer, such as porosity, mean pore radii, structure model index and degrees of anisotropy. Furthermore, permeability of the GDL was obtained through lattice Boltzmann numerical modeling.

1. Introduction

GDL is a heterogeneous porous carbon-based material which allows reactant gases to pass through to the catalyst layer whilst removing any excess liquid water in a polymer electrolyte fuel cell [1]. Although numerous models have been developed to describe the behaviour of GDL in terms of fluid transportation and fuel cell performance, the models are all generally dependant on the use of key parameters such as porosity, mean pore radii, permeability and effective diffusivity which are all determined by the micro/nano structural characteristics of the material. Such parameters cannot be determined without a thorough understanding of the 3D geometry of the real material. In porous electrode theory, such parameters are usually estimated based on idealized models or assumed to be adjustable parameters [2]. In order to accurately understand the structural and material characteristics affect internal flows, it is necessary to generate representative 3D digital models that can be used with pore analysis and numerical flow simulation tools.

NanoCT reconstructs an object by assembling the projected images of an object viewed from different directions. Images are produced based on the level of X-ray attenuation which reflects the density of the sample. These grey scale shadow images are then used to make 2D slices corresponding to what would be seen if the sample is cut through the scanning plane. The slices are then assembled to reconstruct a 3D image. X-ray images can be generated using high resolution microtomography and nanotomography scanners. The former provides a resolution of 1–10 lm, while the later can produce a resolution ┐ 100 nm. Recently, X-ray nanotomography at resolution of 700 nm has been used to determine the two-phase material parameters of a GDL [3–8]. Here, an Xray nanotomographical technique with 680 nm resolution has been used on GDL layers to determine the structural and fluid transportation parameters of a real GDL structure.

2. NanoCT scanning and object reconstruction

In this investigation, a $1 \times 1\text{mm}^2$ GDL sample was scanned in front of an X-ray source with 25 kV and 200 μA with a rotation step of 0.5° at a voxel resolution of 680 nm. Four hundred X-ray shadow images were acquired within 40 min. The tomography images were then processed using CTAN software to reconstruct a 3D digital model of the sample, as shown in Fig. 1a [9]. Fig. 1b and c show a typical shadow and a reconstructed cross section image of a carbon cloth GDL. Fig. 1d is a typical binary image of Fig. 1c that is used for the following analysis.

A threshold is applied on the 2D greyscale image slices, which are composed of up to 256 shades of grey. The threshold was finely tuned by comparing the surface of the 3D image obtained by X-ray tomography with a reference scanning electron microscopy (SEM) image of the same surface in terms of average fibre size and connectivity [10].

3. Structural parameters acquisition

A key parameter to determine the capacity of gas and water circulation in the GDL is porosity ε defined by the ratio of pore volume over total volume. A GDL should be sufficiently porous to allow the

flow of reactant gas and water and should be electrically and thermally conductive and adequately rigid to support the membrane electrolyte assembly. Porosity calculation involves two steps: (1) Fine tuned threshold is applied to the reconstructed grey scale images and the binary images are created. In each binary image 0 and 1 represent void space and solid space, respectively. (2) A cubic matrix of those images is built and the ratio between the number of zeros and the total number of elements in the matrix is obtained as the porosity of the GDL layer.

The anisotropy in porous media properties was found to be the most important factor of mechanical strength [11]. Isotropy (or anisotropy) is a measure of 3D symmetry or the presence (or absence) of preferential alignment of structures along a particular directional axis. In a complexly structured volume containing void and solid, if the volume is isotropic, then a straight line passing through the volume at any orientation will make a similar number of intercepts through the solid phase. GDL could be anisotropic, since lines going along the direction of filaments would make few intercepts while lines crossing at right-angle to the direction of the majority of the filaments would make many intercepts, referring to Fig. 1a. Degrees of anisotropy calculated in this way vary from 0 (fully isotropic) to 1 (fully anisotropic).

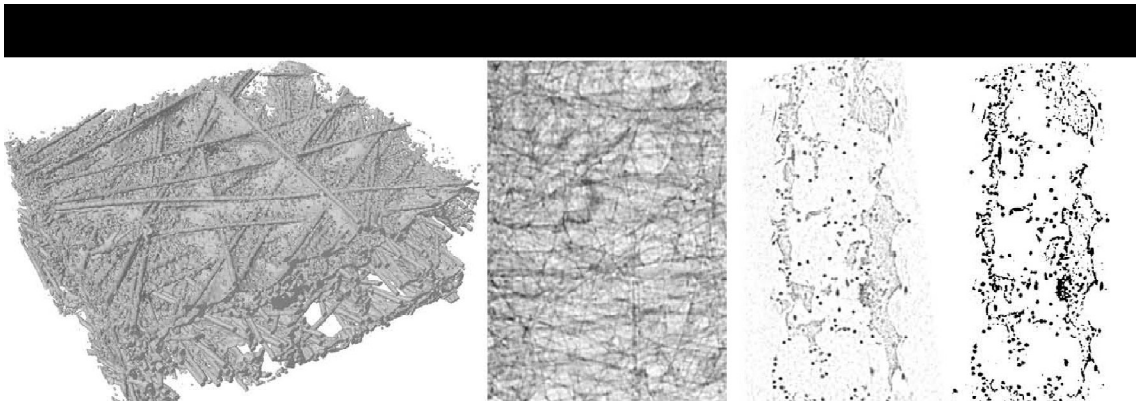

Fig. 1. 3D and 2D images of a GDL carbon paper sample. (a) An isometric view of the reconstructed image of GDL sample with 680 nm resolution using CTAN; (b) a shadow X-ray tomographic image; (c) a 2D reconstructed slice image in grey scale; (d) a binary image of the cross section shown in (c).

Structure model index indicates the relative prevalence of rods and plates in a 3D structure. An ideal plate, cylinder and sphere have values of 0, 3 and 4, respectively [9].

Mean pore radius is an important parameter in GDL characterization as Knudson diffusion is a linear function of the mean pore radius [2]. In the analysis of the 3D images produced using NanoCT a 3D spherical local radius can be measured [12]. Local radius for a point in solid/pore is defined [13] as the radius of a sphere with two conditions: (1) the sphere encloses the point; (2) the sphere is entirely bounded within the solid/pore surfaces.

The above parameters have been calculated directly from the voxel representation through CTAN software based on a sample volume of $300 \times 700 \times 900$ μm^3 with a 680 nm resolution. Porosity and

degrees of anisotropy were found to be 84.1% and 0.91, suggesting that the structure is highly porous and highly anisotropic at micron scale. Structure model index shows that the GDL can be modelled as rods since the index is 2.85. The mean pore radius was obtained as ~8 μm.

4. Fluid transport parameters

Permeability is a material property that describes the ease of the flow within the pore space of a medium. It is of great importance to determine the flow characteristics of the GDL. With the LB method it is relatively facile to deal with complicated boundaries and various forces at microscopic scales and overall therefore it becomes more efficient to simulate complex flows in porous media at pore scale.

The LB method is a numerical model developed over the past two decades to simulate fluid dynamics based on kinetic theory [14,15]. The LB method was designed to overcome some drawbacks of its predecessor, the lattice gas algorithm [16]. It was later found that the LB model can be derived directly from the continuous Boltzmann equation in kinetic theory [17].

The LB model operates by tracking the streaming and collision of a number of fictitious particles in a lattice in terms of particle distribution functions. The particle distribution function $f_i(x,t)$ defines the mass of a particle at location x at time t and moving with velocity ξ_i in the direction i:

$$\frac{\partial f_i(x,t)}{\partial t} + \xi_i \cdot \nabla f_i(x,t) = \frac{1}{\lambda}\left[f_i^{eq}(x,t) - f_i(x,t)\right] \quad (1)$$

where $f_i^{eq}(x,t) - f_i(x,t)$ is the equilibrium distribution function which is the value of $f_i(x,t)$ under an equilibrium state and λ is a relational parameter which controls the rate at which $f_i(x,t)$ approaches $f_i^{eq}(x,t)$.

The LB model considers the particle distribution functions at each voxel in turn and determines a set of nineteen velocities in the 3D spatial domain for the node of each voxel. The nineteen velocities considered are as follow: stagnation at the origin $(0,0,0)/\partial t$; two velocities in the x direction $(\pm\partial x, 0,0)/\partial t$; two in the y direction $(0, \pm\partial x, 0)/\partial t$; four in the x–y plane $(\pm\partial x, \pm\partial x, 0)/\partial t$; four in the y–z plane $(\pm\partial x, 0, \pm\partial x)/\partial t$ and four in the y–z plane $(0, \pm\partial x, \pm\partial x)/\partial t$. This scheme is commonly known as the D3Q19 scheme. The single-phase model assumes that the pores of the GDL are infiltrated by air. Using the detailed velocity field, it is possible to calculate the three components of the permeability tensor for the imaged sample using Darcys law;

$$k_{xx} = \frac{\rho\mu q_x}{(\Delta P/L_x)};\ k_{xy} = \frac{\rho\mu q_y}{(\Delta P/L_x)};\ k_{xz} = \frac{\rho\mu q_z}{(\Delta P/L_x)} \quad (2)$$

where ρ is the density of air, μ is the kinetic viscosity of air, q_i is the average velocity in the direction i, ΔP is the pressure applied in the principal flow direction and L_i is the overall sample length in the direction i. The average velocity q_i is directly related to the velocity field and are obtained by:

$$q_x = \frac{\sum_i u_x(x_i)}{L_x L_y L_z};\ q_x = \frac{\sum_i u_y(x_i)}{L_x L_y L_z};\ q_x = \frac{\sum_i u_z(x_i)}{L_x L_y L_z} \quad (3)$$

where $u_x(x_i)$; $u_y(x_i)$; $u_z(x_i)$ are the three simulated velocity components for each element of the image. Once the absolute permeability is known, the permeability for each specific gas with density ρ_j and kinetic viscosity μ_j can be calculated from $K_j = k/\rho_j\mu_j$. All the variables in Eqs. (2) and (3) are measured in a spatial unit δx and a temporal unit δt. Applying the pressure difference to other two directions allows the other components of the permeability tensor to be calculated.

In the LB model, a pressure difference is applied to two opposite sides of the image along the through-plane direction to drive gas flow. The other four sides at in-plane directions are treated as non-mirrored periodic boundaries, in which two opposite sides are neighboured such that particles moving out of the domain from one side re-enter the domain through its opposite side. All the simulations start from a zero velocity field and the pressure field is linearly distributed in the direction along which the pressure difference is imposed. Steady state conditions are adjudged using the parameter Ω where

$$\Omega = \frac{\sum_i |u_j(x_i t+100) - u_j(x_j,t)|}{\sum_i |u_j(x_j,t)|};\ j = (x,y,z) \quad (4)$$

Flow is assumed to have reached steady state when the tolerance $\Omega < 10^{-5}$ is satisfied.

In the current study, the GDL has a porosity of greater than 80% which thereby eases the computational demand of the LB flow simulation. This therefore allows each voxel of the 3D binary image to be used directly as the lattices of the LB model. In this case, the spatial resolution of the LB model is set equal to the resolution of the X-ray images in the current work.

The LB solver is applied to the fine tuned sample of $100 \times 300 \times 100$ μm^3 (300 μm corresponds to flow direction) to simulate the detailed gas velocity field in the void space of the GDL, with the assumption that the void space is infiltrated by air. The simulated velocity is then used to obtain the absolute permeability for the sample. Because the absolute permeability represents the linear dependence of gas flow rate on pressure gradient, it must be ensured that the flow rate in the simulations is also in this linear range. As such, the pressure difference applied to each region is set to 20 Pa. The simulation is carried out on a dual-core 2.01 GHz workstation with 3.25 GB of RAM. A single-phase simulation for the region takes 500 min. The through plane and in-plane permeabilities (k_{xx}, k_{xy}, k_{xz}) have been found as $4.02 \times 10^{-7}, 5.07 \times 10^{-8}$ and 5.25×10^{-8} mm^2, respectively.

Reference [18] reports a successful study into the combined full morphological reconstruction of fuel cell structures using X-ray computed microtomography with 1.76 μm resolution and lattice Boltzmann modeling to simulate fluid flow at pore scale in a GDL. The validation work demonstrates that the difference between the simulated and measured absolute permeability of air is 3%.

5. Conclusions

Research was conducted on GDL structural parameters which had significant influence to the performance of PEM fuel cells. Structural parameters were obtained after the analysis of the binary images obtained from the nanoCT 3D voxel representation directly.

Fluid transportation parameters reflect the dynamic properties of the GDL and related to the performance of the fuel cells. These parameters were produced based on the binary image of the nanoCT and the analysis using Lattice Boltzmann equation method (LBE). The LBE model was applied to a sample of $100 \times 300 \times 100$ μm (300 μm corresponds to flow direction) to simulate the gas flow through the void space in the GDL. The simulated velocity is then used to obtain the absolute permeability of the image. The through plane and in-plane permeabilities (k_{xx}, k_{xy}, k_{xz}) were found as as $4.02 \times 10^{-7}, 5.07 \times 10^{-8}$ and 5.25×10^{-8} mm^2, respectively.

The current study elucidates the potential to enable improvements in GDL design, material composition and fuel cell design to be realised through a greater understanding of the nano-scale transport processes occurring within the fuel cell.

Acknowledgements

This research was supported by the UK Technology Strategy Board (TSB Project No. TP/6/S/K3032H). We acknowledge industrial partners AVL List GmbH, Intelligent Energy Ltd., Johnson Matthey Plc., Saati Group Inc. and Technical Fibre Products Ltd. for their support of this work.

References

[1] F. Barbir, PEM Fuel Cell: Theory and Practice, Elsevier Academic Press, 2005. pp. 93–99.

[2] A.Z. Weber, J. Newman, Chemical Reviews 104 (2004) 4679–4726.

[3] W.S. Haddad, I. McNulty, J.E. Trebes, E.H. Anderson, R.A. Levesque, L. Yang, Science 266 (1994) 1213–1215.

[4] I. McNulty, Proceedings of the SPIE 4499 (2001) 23–28.

[5] E. Zschech, W. Yun, G. Schneider, Applicd Physics A: Materials Science and Processing 92 (2008) 423–429.

[6] I. McNulty, W.S. Haddad, J.E. Trebes, E.H. Anderson, Review of Scientific Instruments 66 (2) (1995) 1431.

[7] A. Sasov, Proceedings of the SPIE 5535 (2004) 201–211.

[8] J. Becker, V. Schulz, A. Wiegmann, Journal of Fuel Cell Science and Technology 5 (2) (2008) 021006-1–021006-9.

[9] Skyscan Microtomography, CT-Analyser Users Guide, Version 1.6.1, 2007, pp. 19–40, 61–65.

[10] H. Ostadi, K. Jiang, P.D. Prewett, Micro and Nano Letters 3 (4) (2008) 106–109.

[11] A. Odgaard, Bone 20 (6) (1997) 315–328.

[12] D. Ulrich, B. van Rietbergen, A. Laib, P. Rüegsegger, Bone 25 (1999) 55–60.

[13] T. Hildebrand, P. Ruegsegger, Journal of Microscopy 185 (1997) 67–75.

[14] H. Chen, S. Chen, W.H. Matthaeus, Physical Review A 45 (1992) R533–R5342.

[15] G.R. McNamara, G. Zanetti, Physical Review Letters 61 (20) (1988) 2332–2335.

[16] U. Frisch, B. Hasslacher, Y. Pomeau, Physical Review Letters 56 (1986) 1505– 1508.

[17] X. He, L. Luo, Physical Review E 55 (1997) 6333–6336.

[18] P. Rama, Y. Liu, R. Chen, H. Ostadi, K. Jiang, X. Zhang, R. Fisher, M. Jeschke, ASME Journal of Fuel Cell Science and Technology 7 (1) (2010) 1–10.